Electronic Supplementary Material (ESI) for Chemical Communications.

A highly efficient magnetically confined ion source for real time on-line monitoring of trace compounds in ambient air

Ⅰ. Experimental setup

A. Experimental arrangement

The scheme is shown in S1. This ion source consists of three parts, i.e., a micro-fabricated direct current (DC) discharge unit, a Helmholtz coil array, and a ring bias electrode (See S1(a)). The main body of the micro-fabricated DC discharge unit is a hollow cuboid made by ceramic with the inner gas channel sized 25.0 mm (length) ×2.0 mm (width) ×0.7 mm (height) and the exterior sized 25.0 mm ×10.0 mm ×2.7 mm. Inside the ceramic chamber, 1.5 mm apart from the gas outlet, two $3\ \mathrm{mm}^2$ platinum slices are set face to face as the electrodes with the electrode spacing $d = 0.7\ \mathrm{mm}$. This short gas gap facilitates the discharge stability. One of the electrodes is connected to a high-voltage DC power supply through a 100 KΩ ballast resistor which is used to limit the discharge current. The other is connected to the ground. Along the Z axis, the feeding gas helium is introduced into the ceramic chamber via the chamber inlet. A mass flow controller (Sevenstar D07-19B) is used to control the helium flow. The gas flows through the discharge space and is ignited when the voltage applied on the electrode is high enough. Plasma ejects out from the chamber outlet and propagates along the transport path, showing us a plasma plume. The plasma plume was imaged with a digital camera (Nikon D90). The gas temperature of plasma plume was determined by an infrared thermometer (Fluke 63 IR FlexCam) just set out of the chamber outlet. The optical emissions from the plasma plume were obtained through a spectrometer (Ocean Optics HR2000+) with its fiber probe placed at 2.0 cm and perpendicular to the chamber outer surface. During the DC discharge, the gas flow characteristic along the transport path was examined by schlieren imaging through a "Z-type" schlieren system.

The Helmholtz coil array is composed of two same and coaxial tandem coils (I and II) with the radius of 80 mm and width of 12 mm, on the central axis of which the micro-fabricated DC discharge unit is set. The distance between the two coils is 80 mm and the coil II is downstream 20 mm far from the chamber outlet. When the Helmholtz coil array is powered by a second DC power supply with the maximum output voltage of 30 V and maximum output current of 10 A, a longitudinal (parallel to the Z axis) magnetic field B is generated to improve the ion transport efficiency of the ion source. This magnetic field was measured through a Gauss meter with the probe positioned perpendicular to the Z axis.

A steel ring with the optimized dimensions of 17 mm in i.d., 28 mm in o.d., and 2 mm in thickness is used as the bias electrode (with respected to the ground electrode (or the cathode)). This ring bias electrode is set coaxially with the Helmholtz coils and downstream 8 mm away from the chamber outlet. When charged by another home-made electrostatic power supply with the output voltage ranging from -1000 to 1000 V, this ring bias electrode generates an electrostatic field E_r to extract charged particles from the plasma plume. The field spatial distribution was obtained by solving Poisson equation. The charged-particle extraction was examined by observing the variation of plasma plume current with the bias potential in the case of no magnetic field and no sampling. The plume current was measured by a weak current detector (HB-821).

B. Operational procedure

S1(b) shows the operational procedure. A liquid sample is injected into the plasma plume at a rate of 0.1 μL/min through syringe pump. The syringe is set downstream 1 mm away from the chamber outlet. Reactive species R^{g} in the plasma plume reacts with the sample (solvent X and solute M) and ambient vapor ($\mathrm{H_2O}$), accompanied by the production of molecule ions ($[\mathrm{M+W}]^+$). The molecule ions extracted by the electrostatic field E_r are confined in the transport path by the longitudinal magnetic field B and flow into the analyzer inlet due to the gas flow. The analyzer inlet is set on the central axis of the Helmholtz coils and downstream 5 mm away from the coil II. The radius R_a of the analyzer inlet is 2 mm and the distance l between the analyzer inlet and the chamber outlet is 25 mm. A commercial ion trap mass spectrometer (LCQ Fleet, Thermo fisher, San Jose, CA) is employed as analyzer to verify the performance of the ion source. This mass spectrometer is equipped with Xcalibur software (version 1.4RS1) as the corresponding workstation. The mass spectra were recorded under automatic gain mode with the maximum ion injection time of 100 ms set at 3 microscans per spectrum.

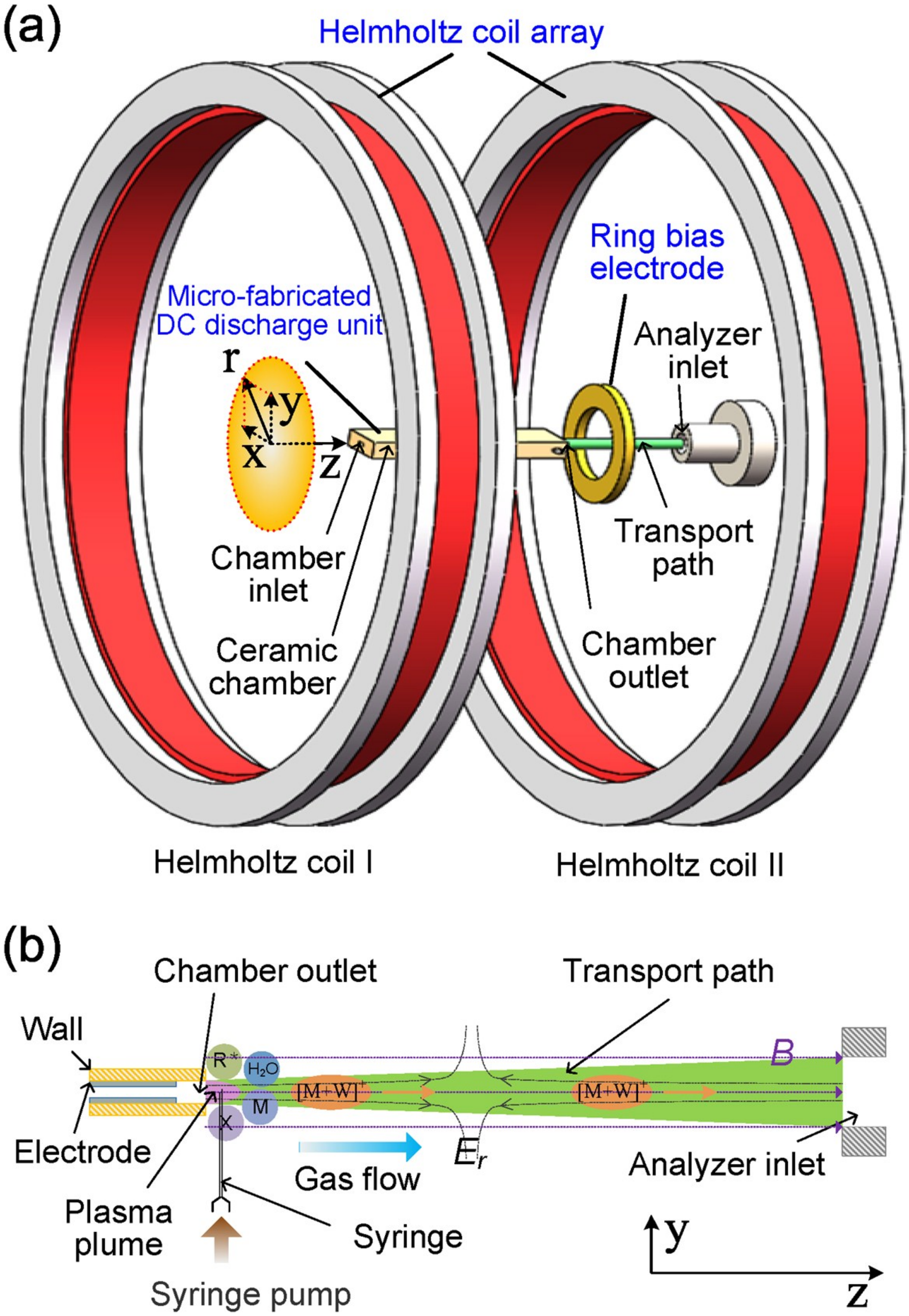

S1. The schamatic diagram of (a) experimental arrangement and (b) operational procedure. (Corresponding to Fig. 1 in the article file)

Ⅱ. Electric and magnetic characteristics of the ion source

S2(a) shows the voltage-current characteristic of the micro-fabricated DC discharge, together with the relationship between the gas temperature and the discharge current. The helium gas flow is set at 1.2 L/min. In the discharge current scope of 2 to 20 mA, the discharge voltage increases with the current, indicating that the DC discharge works in abnormal glow mode, where a relatively high-level ionization occurs. The gas temperature also rises with the current and reaches nearly 80℃ at 20 mA. The magnetic field in the central region of the Helmholtz coil array was examined with the increasing current that passes through the coils. A directly proportional relationship is observed in S2(b). The magnetic field is 50 Gs at the rated current of 4.5 A.

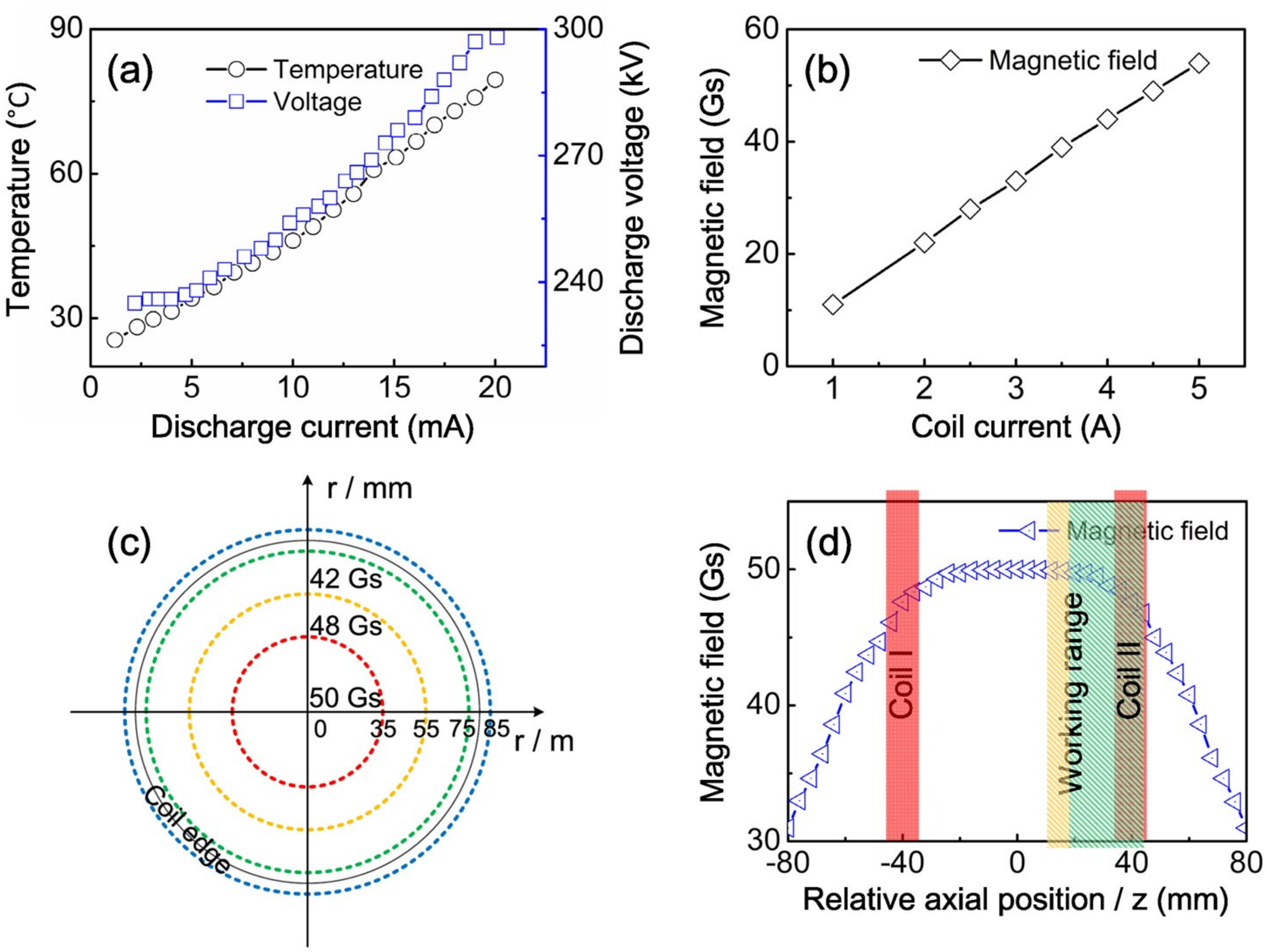

S2. (a) The gas temperature and discharge voltage as a function of discharge current, (b) the variation of magnetic field in the central region of the Helmholtz coil array with the coil current, (c) the radial distribution of magnetic field in the middle plane of the

Helmholtz coil array with the coil current set at 4.5 A, and (d) the axial distribution of magnetic field of the Helmholtz coil array with the coil current set at 4.5 A.

The radial distribution of magnetic field in the middle plane of the Helmholtz coil array was also examined at the rated current, with the result shown in S2(c). It is found that the magnetic field spreads uniformly (with the value of 50 Gs) in the circular region with the radius no more than 35 mm and gradually diminishes along the radial direction outwards. S2(d) shows the axial distribution of magnetic field of the Helmholtz coil array at the rated current, where the central point of the Helmholtz coil array is designated as the coordinate origin. With respect to the coordinate origin, the magnetic field takes a symmetrical profile with the value in the center higher than that at the edges and it approximately remains constant 50 Gs in the range of $-20\ \mathrm{mm} \leq z \leq 20\ \mathrm{mm}$. When z approaches $\pm 40\ \mathrm{mm}$, the magnetic field declines to 47 Gs. The two red straps indicate the place where the two Helmholtz coils are set. The yellow shadow strap means the region where the DC discharge occurs. The green shadow strap indicates the transport path, in which the charged particles are transported.

III. Determination of the bias potential

In our experiment, a ring bias electrode is employed to extract desirable charged particles from the plasma plume and focus them along the transport path directed to the inlet of the analyzer. The signal intensity of sample and the signal intensity enhancement due to the magnetic field are both dominated by the bias potential U_{bias} applied on the electrode. Here, salicylic acid was selected as a sample to investigate the influence of the bias potential on the signal intensity and the signal intensity enhancement. The salicylic acid was prepared in aqueous solution and pumped into the helium gas channel with the concentration of 2.6 ng/ml. The mass spectrometer was operated in the positive ion mode. The variations of the mass spectral intensity of the molecule ion at m/z 138 and the total ion current (TIC) with the bias potential are shown in S3(a) and S4(a), respectively. It is found that a similar or same profile evolution is observed for the TIC and the spectral intensity of the typical molecular ion in the case of a 50

Gs magnetic field applied. S3(a) and S4(a) both show that the MS signal gradually decreases during the bias potential from 0 to 400 V and becomes steady beyond 400 V with the magnetic field applied or not. When the bias potential is negative with the magnetic field applied, the MS signal first drops quickly and reaches its local minimum at -200 V. Then it slowly falls to zero at -900 V after a small magnitude of rise. In the case of no magnetic field, the MS signal is reduced on the whole and tends to be zero at -600 V. Further observation shows that the MS signal intensity at 50 Gs is absolutely higher than that at 0 Gs during the bias potential from -600 to 600 V.

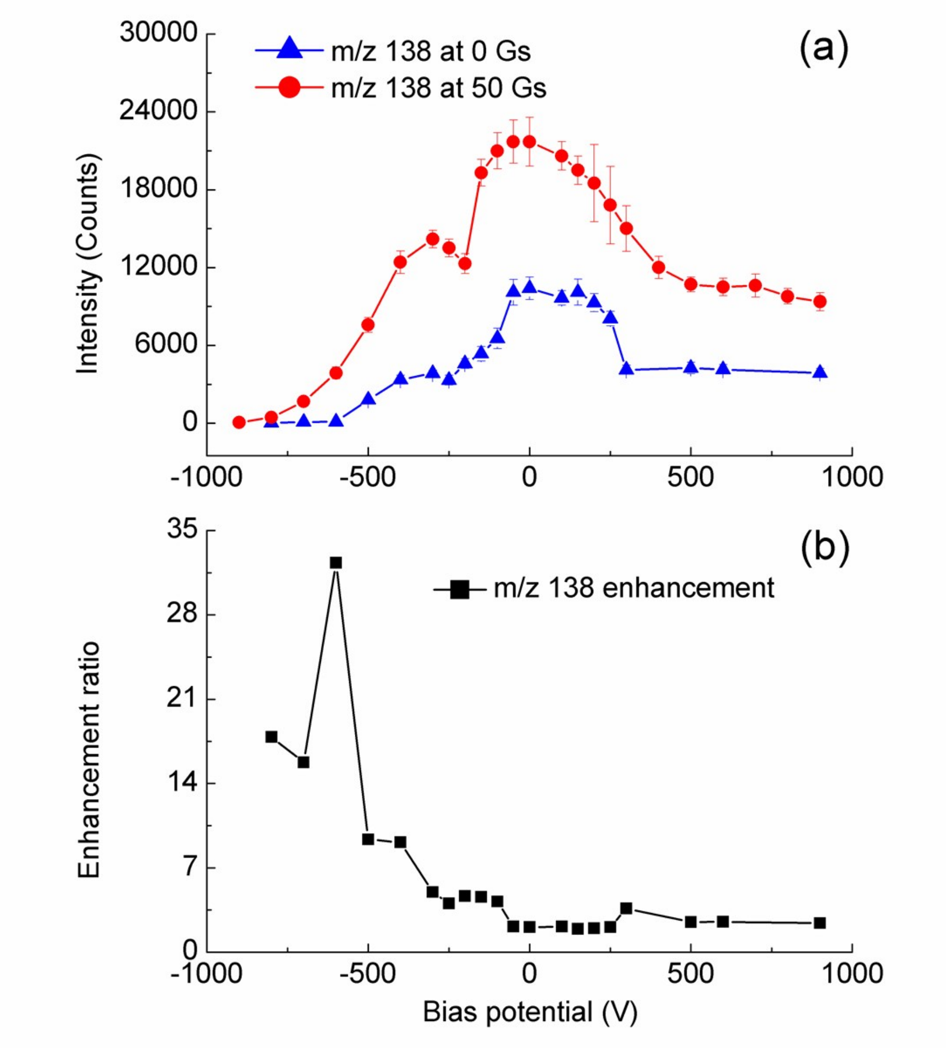

S3. Plots of (a) the mass spectral intensity and (b) the spectral intensity enhancement ratio of the molecular ion at m/z138 as a function of bias potential applied to the ring bias electrode. He flow rate was set at 1.2 L/min.

The MS signal enhancement ratio with a 50 Gs magnetic field applied was obtained by comparing the red and blue curves, with the results shown in S3(b) and S4(b). When the bias potential varies from 400 to -50 V, the signal enhancement is about 2 times for both the TIC and the mass spectral intensity of the typical molecule ion. However, the enhancement ratios increase rapidly with the bias potential further decreasing. The largest enhancement ratio is obtained at -600 V (32.3 for the molecular ion at m/z 138) and -500 V (53.6 for TIC), but where the mass spectral intensity is much lower than that at 0 V.

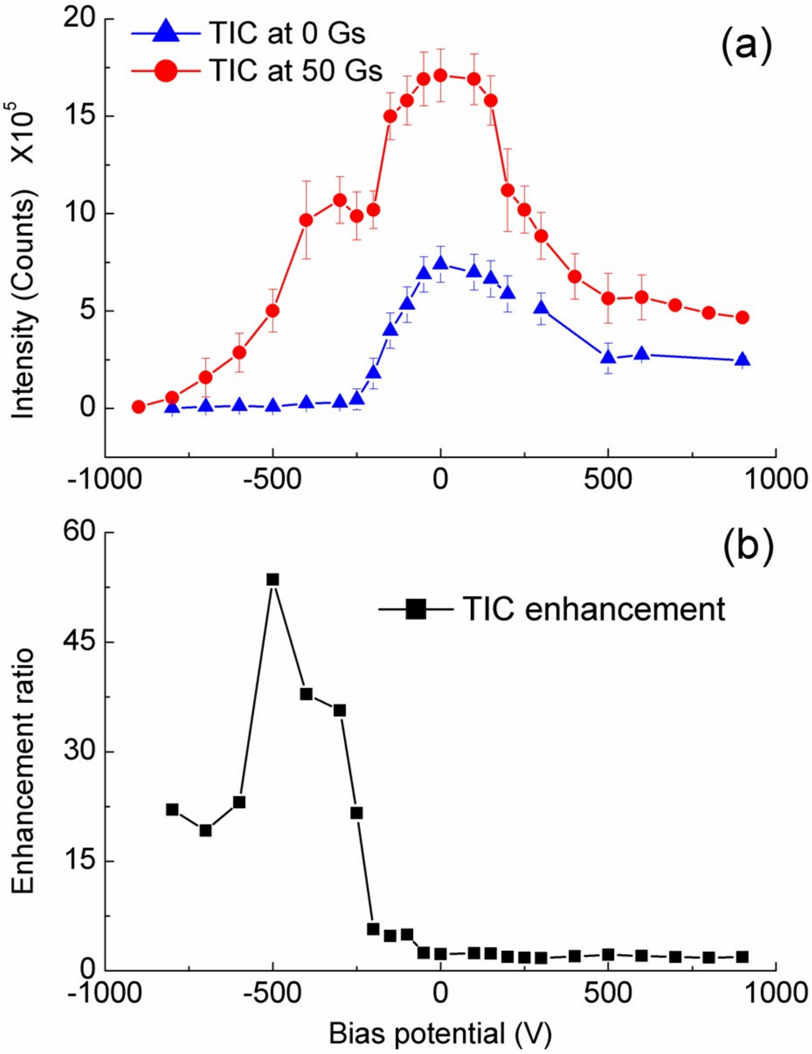

S4. Plots of (a) the TIC and (b) the TIC enhancement ratio as a function of bias potential applied to the ring bias electrode. He flow rate was set at 1.2 L/min.

In order to avoid the MS signal loss caused by a high bias potential as far as possible, we should consider the signal intensity and the signal intensity enhancement together. Finally, an optimized U_{bias} of -100 V is chosen for the following sample analysis. At this bias potential, a 5-fold signal enhancement is achieved for both the TIC and the molecular ions at m/z138.

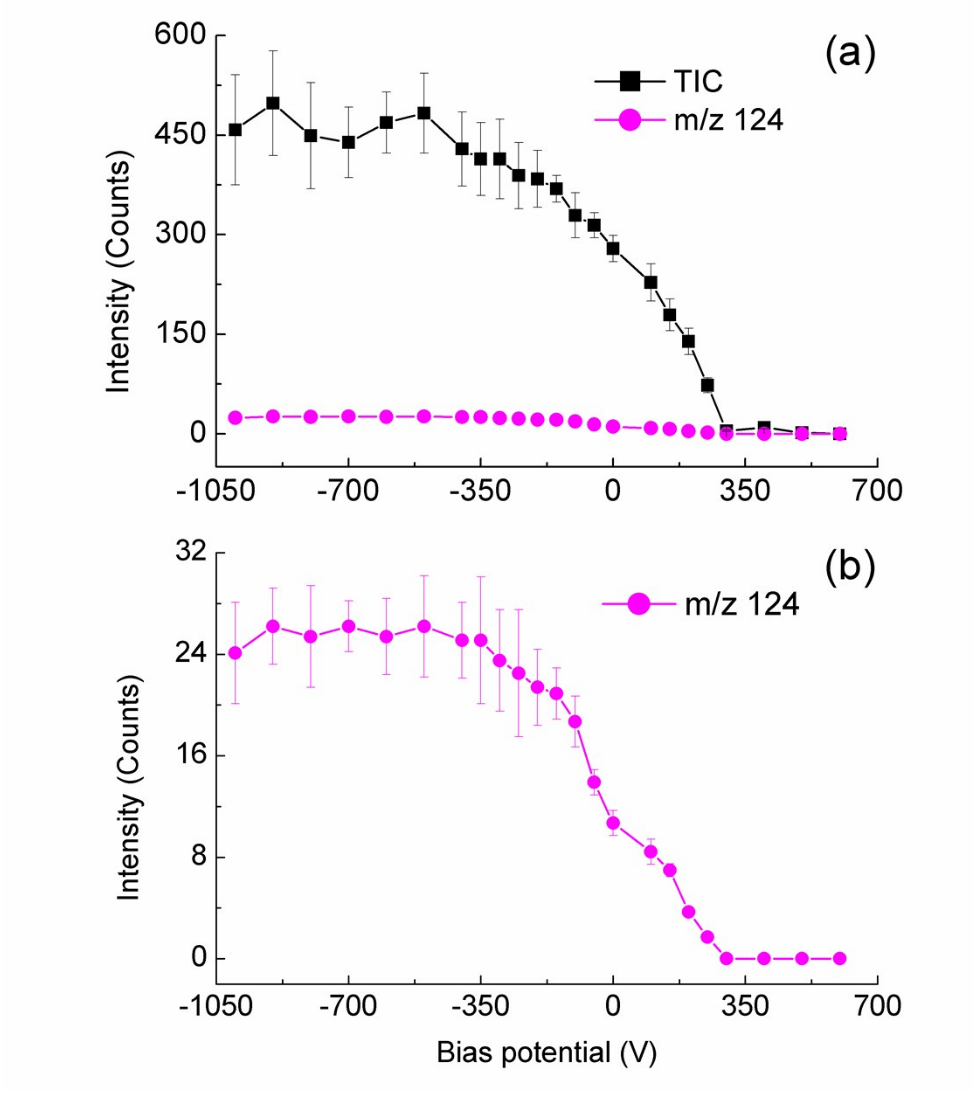

S5. (a) Plots of the TIC and the mass spectral intensity of the molecular ion at m/z 124 as a function of bias potential applied on the ring bias electrode. He flow rate was set at 1.2 L/min. The profile evolution of the mass spectral intensity of the molecular ion at m/z 124 is enlarged in (b).

When the mass spectrometer was operated in the negative ion mode, the variations of the TIC and the mass spectral intensity of the molecule ion at m/z 124 (for salicylic acid) with the bias potential were also examined and the results are shown in S5. It is found that the MS signal remains at a higher level and changes little when the bias potential is less than -400 V. With the bias potential increasing beyond -400 V, the MS signal drops rapidly and tends to be zero at 400 V. However, it should be noted that the mass spectral intensity in the negative ion mode is rather low compared with that in the positive ion mode, because the mass spectrometer is not so powerful for negative ion detecting. Therefore, the subsequent experiments are mainly fulfilled in the positive ion mode.

IV Background spectra and desorption/ionization mechanisms

A. Formation of the background spectra

The background mass spectra of helium and argon plasmas were examined with the results shown in S6(a) and S6(b), respectively. Here, the helium gas flow and argon gas flow were both fixed at 1.2 L/min and the discharge current was set at 12 mA, It follows from S6 that for both helium and argon plasmas, several protonated water clusters ($[(H_2O)_nH]^+$ (n = 2−5)) appear in the range of m/z = 20 −100, with $[(H_2O)_2H]^+$ and $[(H_2O)_3H]^+$ dominating the spectra. As for the helium plasma, production of the protonated water clusters could be traced back to the collision between the metastable He^* and N_2 (Penning Ionization):

$$He^* + N_2 \rightarrow He + N_2{}^+ + e,$$

where, N_2 is ionized to $N_2{}^+$ and the energy is finally delivered to water in the ambient air through a chain of reactions.[1] As a result, the water clusters are formed. Since the energy level of metastable Ar* is lower than that of $N_2{}^+$, the same reaction path will not occur in the Ar plasma, resulting in a lower efficiency of ionizing sample molecules. The energy levels of reactive species helium (He* and He^+) and argon (Ar* and Ar^+) are both higher than that of water. The water clusters can also be generated by the direct energy transfer from the He/Ar plasma to water.[2]

$$He^*/Ar^* + (n+1)H_2O \rightarrow He/Ar + [(H_2O)_nH]^+ + OH^-$$

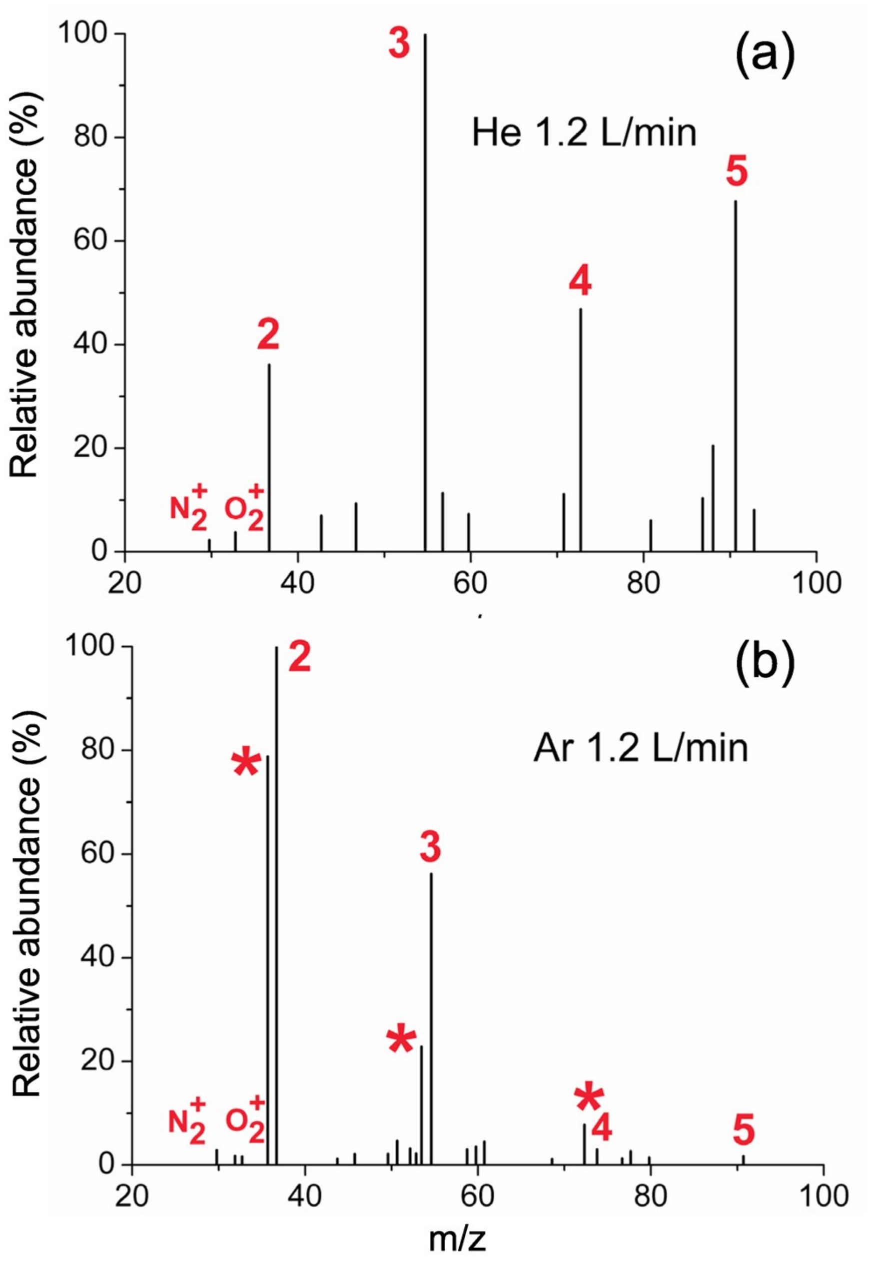

S6. Background mass spectra of (a) the helium and (b) argon plasmas.

From the mass spectrum of Ar plasma, it is also found that several strong peaks marked by "*" are presented. These peaks are conjectured to be $[(H_2O)_nNH_4]^+$ or $(H_2O)_n$,[3] while further study is needed because the mass spectrometer used in our experiment is not so powerful in the low m/z range. The optical emissions from He and Ar plasmas were also examined. S7(a) and S7(b) show the optical spectra of He and Ar plasmas, respectively. The presence of OH, N_2, NO, and OI suggests that the charge transfer (O^+, O_2^+, NO^+, and N_2^+) also occurs in the ionization process in He or Ar plasma, aside from the proton transfer ($[(H_2O)_nH]^+$).

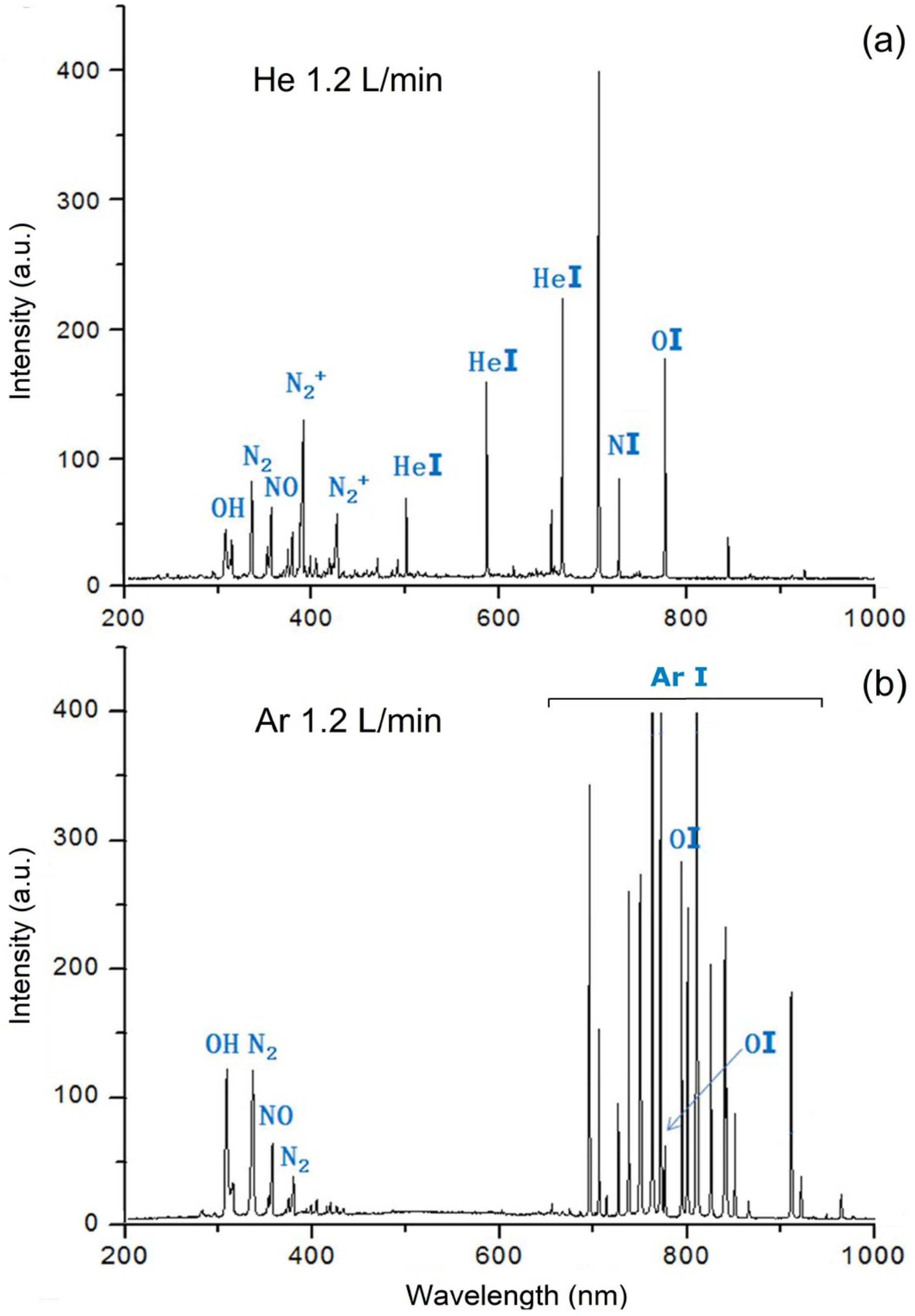

S7. Optical emission spectra of (a) the helium and (b) argon plasmas.

B. Desorption/ionization mechanisms in the sampling process

In our experiment, under the condition that the helium (or argon) gas flow was fixed at 1.2 L/min and the discharge current was set at 12 mA, the plasma plume temperature was examined to be about 45°C for helium (S2(a)) and 65°C for argon (not shown here). The low-temperature nature suggests the possibility of nonthermal momentum desorption in the sampling process. The background mass spectra show amounts of water clusters are produced in the plasma. These water clusters play a key role in protonization of the sample molecules following this way: [4]

$$[(H_2O)_nH]^+ + M \rightarrow nH_2O + [M + H]^+.$$

In addition to ionizing the sample molecules by the proton transfer from the water clusters in the sampling process, the metastable He^* can directly interact with the sample molecules due to its high energy level, and produce molecular ions:[5]

$$He^* + M \rightarrow He + M^+ + e.$$

For some samples containing functional groups (such as hydroxyl, carboxyl, and ester group), molecular ions (e.g., $[M\text{-}OH]^+$ and $[M\text{-}CH_3COO]^+$ are probably produced by detaching these functional groups from the matrix due to the collisions with reactive species. These detached functional groups are converted into water and acid through recombination with the water clusters. Subsequently, combining the water and acid with M^+ leads to the formation of the adduct ions, such as $[M+H_2O]^+$ and $[M+CH_3COOH]^+$. The mechanisms proposed above can be verified by observing molecular ions (e.g., M^+, $[M+H]^+$, $[M+H_2O]^+$, and $[M+CH_3COOH]^+$) in the positive-mode mass spectrum, which have been addressed in the main body. The corresponding transformation probabilities depend on the size and structure of the molecule concerned and its chemical environment. A similar or same discussion on the formation of molecular ions has been made in these references (*Angew. Chem. Int. Ed., Engl.*, 1994, 33, 1023–1043; *Mass Spectrom. Rev.*, 2017, 36, 423–449; *Anal. Chem.*, 2017, 89, 3191−3198; *Anal. Methods*, 2017, 9, 5065–5074). Although probable chemical reaction paths are demonstrated for the formation of the typical molecular ions, CID examination is required to make the chemical reaction processes more clear in the future.

V. Verifying the magnetic confined ion source by mass spectrometric detection of typical samples

A. Test sample examination

In the main body, we demonstrate the improvements of MS signal intensity and detection sensitivity of the aspirin solution in detail, which shows a high performance of the magnetic confined ion source but only for a typical sample. To verify the performance of the ion source in a larger application area, more samples are examined, where the samples are pumped into the gas channel with different concentrations. Here, the helium gas flow was fixed at 1.2 L/min, the discharge current was set at 12 mA, and the bias potential was adjusted to -100 V. S8(a) and S8(b) show the mass spectra of methyl salicylate (1.5 ppm) with and without magnetic field, respectively. Here, it should be noted that the ordinate scale in S8(a) is approximately 10 times of that in S8(b).

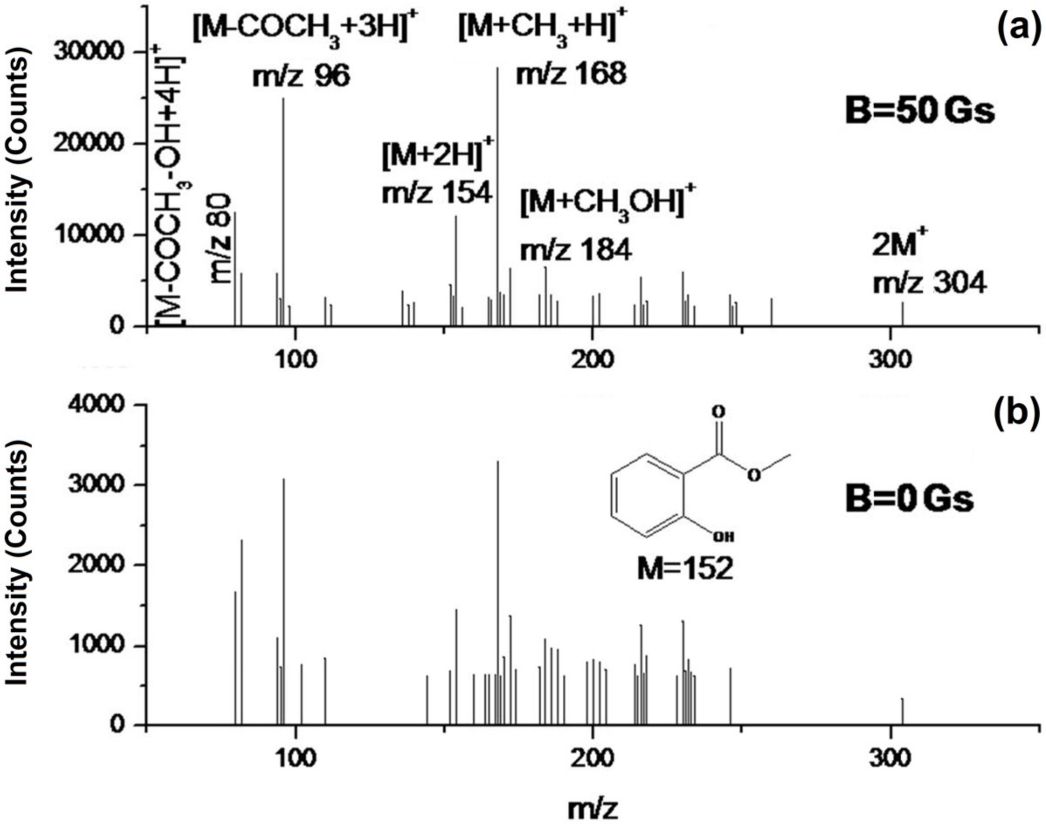

S8. Mass spectra of 1.5 ppm methyl salicylate (a) with the magnetic field of 50Gs and (b) without magnetic field.

From S8, it can be seen that several mass spectral lines, corresponding to the molecular ions m/z 80 [M-$COCH_3$-OH+4H]$^+$, m/z 96 [M-$COCH_3$+3H]$^+$, m/z 153 [M+H]$^+$, m/z 154 [M+2H]$^+$, m/z 168 [M+CH_3+H]$^+$, m/z 184 [M+CH_3OH]$^+$, and m/z 304 2M$^+$, are observed in both the cases. With the magnetic field of 50 Gs applied, the mass spectral intensity of the molecular ion m/z 154 [M+2H]+ increases from 1445 to 12187 counts and an approximate 8-fold enhancement in the signal intensity is obtained. Other molecular ions, such as m/z 153 [M+H]$^+$, m/z 168 [M+CH_3+H]$^+$, m/z 184 [M+CH_3OH]$^+$, and m/z 304 2M$^+$, also show a 6- to 9-fold enhancement of spectral intensity (See Table 1). When the ion m/z 154 $[M+2H]^+$ was selected as indicator, the LoD (at S/N=3) was examined to be 128 ppb and 15 ppb without and with the 50 Gs magnetic field applied, respectively, indicating a great improvement (~9 times) in the detection sensitivity due to the applied magnetic field. Here, five groups of parallel tests were used for obtaining more accurate and more reproducible experimental results.

Table 1. Comparison of the mass spectral intensity of various molecular ions for the sample methyl salicylate with and without a 50 Gs magnetic field applied.

Detected ion (Mass charge ratio) (Molecular ion)	**Mass spectral intensity at 0 Gs / Counts** (Uncertainty[a])	**Mass spectral intensity at 50 Gs / Counts** (Uncertainty[a])	**MS signal enhancement ratio[b]** (50 Gs / 0 Gs)
m/z 80 $[M-COCH_3-OH+4H]^+$	1670 (124)	12574 (2334)	X7.5
m/z 96 $[M-COCH_3+3H]^+$	3092 (290)	25070 (1520)	X8.1
m/z 153 $[M+H]^+$	422 (28)	3413 (764)	X8.1
m/z 154 $[M+2H]^+$	1445 (225)	12187 (1392)	X8.4
m/z 168 $[M+CH_3+H]^+$	3311 (441)	28309 (1019)	X8.6
m/z 184 $[M+CH_3OH]^+$	1093 (190)	6604 (568)	X6.0
m/z 304 $2M^+$	290 (78)	2630 (391)	X9.1

[a] Referring to the uncertainty of recorded mass spectral data.

[b] Ratio of the arithmetic mean values.

The performance of the magnetic confined ion source for mass spectrometric detection of other samples is summarized in Table 2 and Table 3. The samples include ethanol, acetonitrile, 1, 4-dioxane, toluene, diethyl ether, hexane, and ethyl acetate. These samples were monitored under the same conditions as stated above. From Table 2, it is found that application of 50 Gs magnetic field at least gives rise to a 3-fold enhancement in the signal intensity, when the 1,4-dioxane is used as sample and the molecular ion m/z 102 $[M+H-OH+CHO]^+$ is selected as indicator. In the examination of hexane, a 20-fold signal enhancement is achieved for the molecular ion m/z 100 $[M+CH_2]^+$.

Observation of the monitoring results of all the samples indicates that the mass spectral intensity of molecular ions increases about 10 times for most of the samples.

The performance of the magnetic confined ion source for mass spectrometric detection has also been verified in the working gas argon, with the results shown in Table 2. Here, the gas flow was still fixed at 1.2 L/min. The discharge current was 12 mA and the bias potential was -100 V. In this case, the MS signal enhancement ratio is less than 10 for most of the samples and a greater signal enhancement is obtained only for the toluene, where the molecular ions m/z 94 $[M+2H]^+$ and m/z 108 $[M+CH_3+H]^+$ are selected as indictor.

Table 2. MS signal enhancement ratios for various samples with helium and argon respectively used as working gas.

No.	**Sample**	**Sampling concentration**	**Detected ion** (Mass charge ratio, molecular ion)	**MS signal enhancement ratio** (50 Gs / 0 Gs)^{a,b}	
				He	Ar
1	Ethanol	492.5 ppb	m/z 47 $[M+H]^+$	X9	X6
			m/z 74 $[M-H+CH_3CH_2]^+$	X18	X8
2	Acetonitrile	493.8 ppb	m/z 42 M^+	X5	X4
			m/z 44 $[M+2H]^+$	X4	X4
			m/z 83 $[2M-H]^+$	X7	X6
3	1,4-dioxane	650 ppb	m/z 87 $[M-H]^+$	X5	X3
			m/z 102 $[M+H-OH+CHO]^+$	X3	X3
4	Toluene	1.1 ppm	m/z 91 $[M-H]^+$	X10	X4
			m/z 94 $[M+2H]^+$	X11	X10
			m/z 108 $[M+CH_3+H]^+$	X15	X15
5	Diethyl ether	266 ppb	m/z 74 M^+	X4	X4
			m/z 75 $[M+H]^+$	X5	X4
			m/z 88 $[M+CH_2]^+$	X13	X5
6	Hexane	865 ppb	m/z 86 M^+	X12	X8
			m/z 100 $[M+CH_2]^+$	X20	X5
7	Ethyl acetate	562.5 ppb	m/z 89 $[M+H]^+$	X6	X6

[a] The values in this row are approximately integers of the precise ratios.

[b] Ratio of the arithmetic mean value of the MS signal.

Comparing the monitoring results in the two working gases indicates that the enhancement ratio is always higher (or no less than) for the helium than for the argon gas. This means that the helium plasma contributes more to the MS signal enhancement than the argon plasma. This phenomenon is mainly resulted from the fact that the metastable He* (18.4–20.6 eV) is more energetic than the metastable Ar* (~11.5 eV) and the helium plasma has a higher efficiency in ionization of the samples. Thus, we claim that the performance of the magnetic confined ion source also correlates with the charged species produced in the plasma and that the charged species play a key role in the ionization process.

The LoD was also examined for these samples, with the results shown in Table 3. Here, helium was employed as working gas with the flow rate set at 1.2 L/min. The discharge current was 12 mA and the bias potential was -100 V. To determine the LoD, a molecular ion was selected as indicator for each sample. It follows from Table 3 that the LoD with a 50 Gs magnetic field applied is reduced to 1/3 of that in the case of no magnetic field for these samples, such as diethyl ether and hexane. When the samples ethanol, acetonitrile, 1,4-dioxane, and ethyl acetate are concerned, the LoD can be lowered to 1/4–1/7 of the original level. For the sample toluene, the molecular ion m/z 91 $[M-H]^+$ was served as indicator and the LoD was reduced from 700 to 72 ppt with the magnetic field applied. In this case, a substantial improvement (about 10 times) is achieved in the detection sensitivity of MS.

Table 3. Reduction of LoD for various samples due to the application of 50 Gs magnetic field.

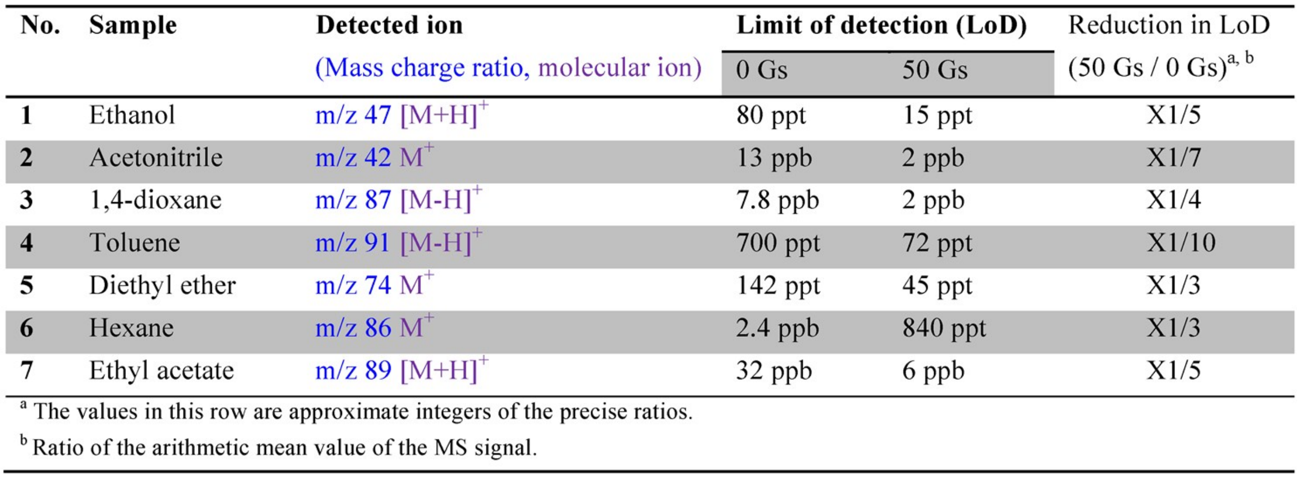

No.	**Sample**	**Detected ion** (Mass charge ratio, molecular ion)	**Limit of detection (LoD)** 0 Gs	 50 Gs	Reduction in LoD (50 Gs / 0 Gs)$^{a, b}$
1	Ethanol	m/z 47 $[M+H]^+$	80 ppt	15 ppt	X1/5
2	Acetonitrile	m/z 42 M^+	13 ppb	2 ppb	X1/7
3	1,4-dioxane	m/z 87 $[M-H]^+$	7.8 ppb	2 ppb	X1/4
4	Toluene	m/z 91 $[M-H]^+$	700 ppt	72 ppt	X1/10
5	Diethyl ether	m/z 74 M^+	142 ppt	45 ppt	X1/3
6	Hexane	m/z 86 M^+	2.4 ppb	840 ppt	X1/3
7	Ethyl acetate	m/z 89 $[M+H]^+$	32 ppb	6 ppb	X1/5

[a] The values in this row are approximate integers of the precise ratios.

[b] Ratio of the arithmetic mean value of the MS signal.

B. Practical application

Further, filtrate of tobacco leaf was prepared to demonstrate the practicability of the magnetic confined ion source. To obtain the filtrate, 2 g tobacco leaf was taken from a cigarette and soaked in 40 ml methanol for an hour, and then the soak solution was suctionally filtrated in order to remove solid impurities. The filtrate was pumped into the helium gas channel at 0.5 μL/min. The gas flow was 1.2 L/min, the discharge current was 12 mA, and the bias potential was -100 V. S9 shows the mass spectra of the tobacco leaf filtrate with a 50 Gs magnetic field applied or not. The spectral line at m/z 149 is rather high and it corresponds to a protonated molecular ion of phthalic anlydride, which is considered as a common fragment ion of plasticizer in both the tobacco paper and the gas channel. Even so, nicotine, a main ingredient of tobacco, is well distinguished by monitoring the ion $[M+H]^+$ at m/z 163 in both the spectra. Comparing the two cases shows that this ion has a 6-fold enhancement in the spectral intensity, i.e., increasing from 461 counts without magnetic field to 2583 counts with a 50 Gs magnetic field applied. Meanwhile, the spectral line at m/z 79 (a fragment ion of nicotine) was examined to be 1061 and 107 counts with and without magnetic field, respectively, exhibiting a 10-fold improvement in the MS signal.

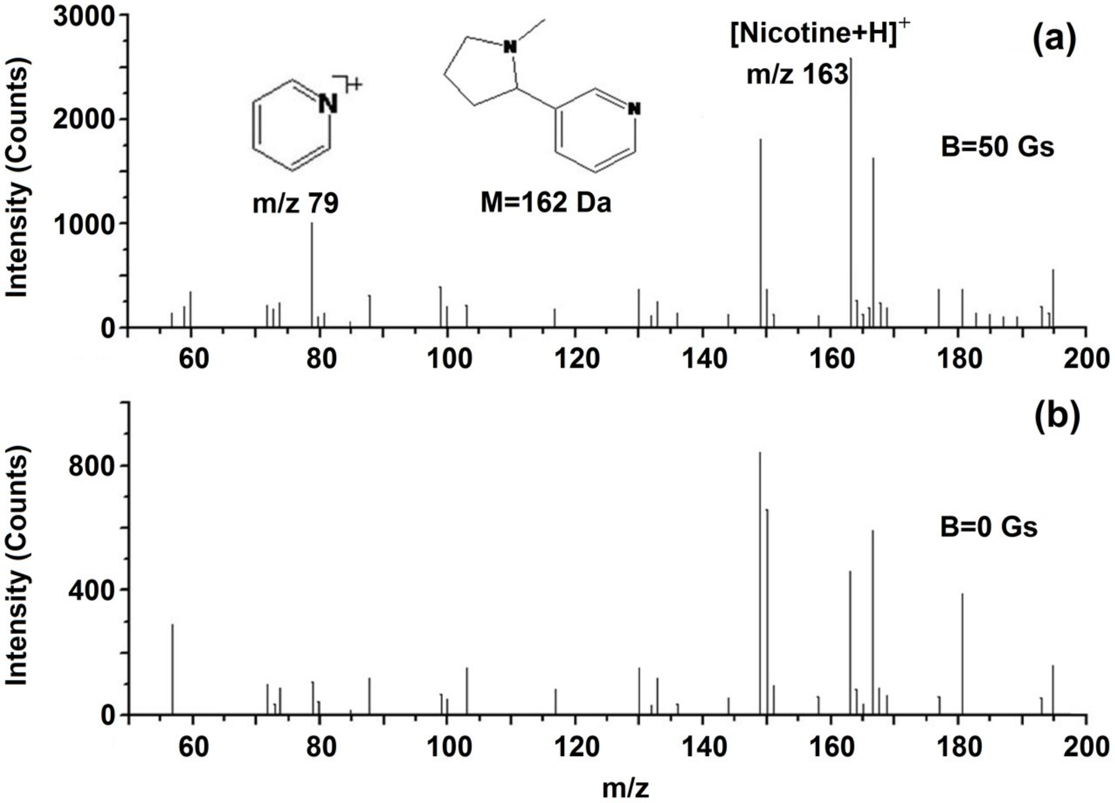

S9. Mass spectra of filtrate of tobacco leaf (a) with and (b) without magnetic field applied.

VI. Comparison of the magnetic confined ion source with its counterparts

Originating from the desorption electrospray ionization (DESI) in 2004, the ambient mass spectrometry has expanded into a big family.[6,7] Several researchers clarified the complicated relations by classifying the majority of members into spray-based and plasma-based techniques.[8,9] It is generally accepted that both parties behave quite similarly for small molecule detection, while the different construction mechanisms induce a subtle difference in applications. For spray-based techniques, applications in bioanalysis are suitable for detecting molecules with a mass up to 66 kDa,[9] while the plasma-based techniques are mostly used for weak-polar and low-mass range molecules.

Plasma-based ambient MS ion sources are currently being investigated by several research groups for rapid identification and semiquantification of samples, such as drugs, foodstuffs and agrochemicals, polymers, chemical warfare agents, and explosives. These techniques include direct analysis in real time (DART), atmospheric solids analysis probe (ASAP), desorption atmospheric pressure chemical ionization (DAPCI), plasma-assisted desorption ionization (PADI), dielectric barrier desorption ionization (DBDI), low-temperature plasma (LTP), flowing atmospheric-pressure afterglow (FAPA), desorption corona beam ionization (DCBI), microhollow cathode discharge microplasma, and microwave induced plasma desorption/ionization source (MIPDI). Using nitrogen, helium, or argon as the carrier gas, the plasma-based ion sources employ electro-discharges to generate plasmas that contain excited/metastable atoms, radicals, and electrons. The plasma plume or afterglow is directed toward the sample surface, allowing simultaneous or sequential ionization and desorption of the analytes. It is hard to distinguish these techniques based on the mechanisms because in almost all of the related studies penning ionization with the metastable He* or Ar*, charge transfer, and proton transfer were considered to play a key role in the ionization process, accompanied by the momentum desorption and optional thermal desorption.[5,10] When coupling these ion sources to a mass spectrometer, various samples were examined. Some research groups have obtained desirable testing results, as listed in Table 4.

Table 4. The performance of traditional ambient ion sources coupled to MS.

Technique	Basic principle	Physic state of sample	Highest mass	LoD / sample	Dynamic range	References
DESI	Analytes ionized through interacting with spray-droplets	Liquid	1.2 kDa	8 mg/L / salicylic acid	10^3	11
		Gas	300 Da	4 μg / TEP vapor	10^2~10^3	12
		Solid	600 Da	1~33 pg/mm^2 / pesticides	10^2~10^3	13
EESI	Analytes ionized through interacting with spray-droplets	Liquid	400 Da	~3.8 μg/L / malachite green	10^3	14
PS	Analytes ionized through interacting with spray-droplets	Solid, liquid	500 Da	0.5~1 ng/mL / methotrexate, chlorpyrifos, and ciprofloxacin	10^5	15
DART	Sample surface is exposed to plasma gas stream	Solid, liquid, gas	1kDa	7 fmol / ethylpalmitate	10^3~10^4	5, 16–18
		Liquid	200 Da	15 pg/mL / trimethyl hosphate	10^3~10^4	19
		Solid	1 kDa	5 mg/kg / genistein, daidzein and glycitein	10^2~10^3	20
		Solid	500 Da	3 μg/kg / acrylamide	10^2	21
		Liquid	1 kDa	1.1 ng	1~10	22
DAPCI	Sample surface is exposed to gaseous reagent species generated by APCI	Solid, liquid	600 Da	3.4 fg/mm^2 / melamine	10^5	23–25
ASAP	Samples are evaporated and ionized by corona discharge	Solid, liquid	700 Da	N.A.	N.A.	26, 27
DCBI	Plasma beam directly interacts with the analyte	Solid, liquid	600 Da	0.4 ng / citalopram	10^3	28, 29
FAPA	Samples are introduced into the flowing afterglow outside the discharge chamber	Solid, liquid, gas	1.2 kDa	0.043 fmol / terbuthlazine	10^4	30–32
PADI	Sample surface is in direct contact with the nonthermal plasma	Solid, liquid	300 Da	20 μmol / angiotensin II	10^2	33, 34
Microplasma	Sample surface is exposed to the effluent microplasma stream	Solid, liquid, gas	500 Da	0.4 ng/mm^2 / loratadine	N. A.	3
DBDI	Analyte is desorbed/ionized by ion bombardment through the plasma sheath produced by DBD	Solid, liquid	400 Da	3.5 pmol/L / alanine	10^2	35, 36
LTP/PPAMS	Plasma plume ejecting from DBD-constructed chamber reacts directly with the samples	Solid, liquid, gas	500 Da	0.6 pg / TNT	10^4	10, 37, 38
MIPDI	Samples are desorbed/ionized directly by the hot plasma stream ejected from the ion source	Solid, liquid, gas	1.2 kDa	0.73 pg/ml / DMF	10^3	39–41

N.A. represents information not available.

In the work published in Analytical Chemistry (*Anal. Chem.*, 2013, 85, 9013−9020),[42] we have reported a novel ambient ion source, i.e., a microfabricated glow discharge plasma (MFGDP), for mass spectrometry. Compared to the traditional ion sources, the microfabricated DC glow discharge ion source has a relatively high number of reagent ions, but which is supported by a simple power supply. In addition, this ion source has some special merits, including low temperature, considerable stability, simple structure, low power, and low cost. When coupling this ion source to a commercial ion trap mass spectrometer (LCQ Fleet, Thermo fisher, San Jose, CA), gaseous, liquid, creamy, and solid samples with molecular weights up to 1.5 kDa could be examined in qualitative and quantitative analysis. As for the quantitative analysis, analytes were first dissolved in water, neat methanol, or methanol: water (1: 1, V/V) to prepare solution samples, and then these samples were analyzed in two different ways. In the first way, the solutions were added into beakers with a volume of 4 mL, and then the beakers were held 2 mm away under the outlet of the ion source by a homemade sliding sampling device. The plasma plume then ejected toward the solution surface with an angle of ca.45°. With respect to the second way, each solution (5 μL) taken by a microsyringe was dropped onto a filter paper to form a circle sized about 2 cm^2 (assuming that drying of the solution would allow for a homogeneous film), and then the filter paper was quickly located between the MS inlet and the ion source, placing the plasma plume in direct contact with the wet circle with an interaction area of ca. 1 mm^2. Upon most occasions, the LoD values were obtained for various samples via the second way. As shown in Table 5, all the LoDs are in the range of pg/mm^2 to fg/mm^2, with most values obtained in He plasma to be lower than those obtained in Ar plasma. Comparing Tables 4 and 5, we can find that the detection sensitivity of the microfabricated DC glow discharge ion source is located at the similar or same level as the traditional ion sources.

To further improve the detection sensitivity of the microfabricated DC glow discharge ion source, we introduce a weak longitudinal magnetic field to the microfabricated DC glow discharge, as demonstrated in this manuscript. The introduction of magnetic field enhances the transport efficiency of ion source through magnetic confinement. Here, we don't directly compare the magnetic confined ion source with the traditional ones because of the deferent samples and different sampling fashions used in numerous research groups. For convenience, a comparison is carried out between the magnetic confined ion source and the microfabricated DC glow discharge ion source that was proposed in our last work.[42] In that work, the ion source was equipped with no magnetic field. The performance of the magnetic confined ion source is verified by examining the MS signal intensity and the LoD of various samples with a 50 Gs magnetic field applied or not. Comparing the testing results in the two cases shows that the MS signal intensity and the detection sensitivity are both improved to a great extent due to the application of magnetic field. For most of the samples, the mass spectral intensity of molecular ions increases about 10 times. Especially for the sample hexane, a 20-fold signal enhancement is achieved at m/z 100 corresponding to the molecular ion $[M+CH_2]^+$. As far as the detection sensitivity is concerned, the LoD is lowered to 1/3−1/10 of the original level. As stated afore, when no magnetic field is applied, the microfabricated DC glow discharge ion source has a detection sensitivity that is comparable to those of other ambient ion sources. Thus, we claim that the magnetic confined ion source possesses a performance superior to most of the ambient ion sources.

It is generally accepted that a high detection sensitivity of MS is likely to give rise to the loss of certain selectivity, especially for monitoring an intended single molecular ion. With respect to the study on a single molecular ion, it is better to maintain a proper selectivity with an acceptable sensitivity. A systematic experimental investigation on a single molecular ion will be carried out with more objective and more pertinence after improving our ion source and operation strategy in the near future. It is expected that the sensitivity can be enhanced to some extent without losing selectivity for the magnetic confined ion source. Since the ion source and the operation conditions (i.e. the model of mass spectrometer, the state and kind of samples, and the fashion of sampling) in our case are quite different from those employed by other research groups, a direct sensitivity and selectivity comparison cannot be properly implemented between ours and others. An alternative way is that a comparative study on the sensitivity and selectivity is carried out under the condition that an ion source coupled to MS is operated with and without magnetic field. Then, a comparative mass spectrometric analysis will be made to verify the improvement of the sensitivity and selectivity and simultaneously clarify the relationship between the sensitivity and selectivity with the magnetic field applied or not.

Table 5. Performance of the microfabricated DC glow discharge ion source for various samples when coupling it to MS.[42]

Sample	**Solvent**	**Measured ion**[a]	**LoD** (Signal-noise ratio)		**RSD**[c] (Sampling times)	
			He	Ar	He	Ar
L-phenylalanine	Water	m/z 166	2.65 pg/mm^2 (S/N=31)	6.25 pg/mm^2 (S/N=29)	13% (8)	14% (8)
L-serine	Water	m/z 106	22 fg/mm^2 (S/N=12)	2.85 pg/mm^2 (S/N=7)	15% (9)	15% (9)
L-leucine	MeOH	m/z 114	25.4 fg/mm^2 (S/N=28)	13.75 fg/mm^2 (S/N=10)	12% (9)	14% (9)
L-glycine	Water	m/z 76	2.3 pg/mm^2 (S/N=11)	8.28 pg/mm^2 (S/N=17	14% (8)	12% (8)
L-alanine	Water	m/z 90	100 fg/mm^2 (S/N=19)	37.5 pg/mm^2 (S/N=10)	16% (8)	13% (8)
Urea	MeOH, Water[b]	m/z 61	2 pg/mm^2 (S/N=13)	0.8 fg/mm^2 (S/N= 16)	14% (8)	17% (8)
Gallic acid	MeOH	m/z 171	5 pg/mm^2 (S/N=31)	46.68 pg/mm^2 (S/N=20)	17% (9)	16% (9)
Ibuprofen	MeOH	m/z 207	1 pg/mm^2 (S/N=65)	10.91 pg/mm^2 (S/N=20)	13% (9)	13% (9)
Paracetamol	MeOH,1:1 MeOH:water[b]	m/z 152	0.25 fg/mm^2 (S/N=46)	15 fg/mm^2 (S/N=12)	15% (8)	16% (8)
Asprin	MeOH	m/z 181	4.75 fg/mm^2 (S/N=42)	47 pg/mm^2 (S/N=18)	11% (10)	12% (9)
Phenacetin	MeOH	m/z 180	40 fg/mm^2 (S/N=18)	10 pg/mm^2 (S/N=13)	14% (10)	17%(10)
Reserpine	MeOH	m/z 609	3.5 pg/mm^2 (S/N=23)	87.5 pg/mm^2 (S/N=20)	20% (8)	14%(8)
Cholesterol	MeOH	m/z 388	800 fg/mm^2 (S/N=10)	23.5 pg/mm^2 (S/N=11)	18% (8)	15% (8)

[a]The measured ion was [M+H]$^+$ for all the analytes. [b]The solvents employed in the He and Ar induced detections were not the same: Ar induced detection was performed with those marked . [c]The RSD value was determined at the corresponding LoD.

References

1. G. Nicol, J. Sunner and P. Kebarle, *Int. J. Mass Spectrom. Ion Processes*, 1988, **84**, 135−155.
2. J. Kratzer, Z. Mester and R. E. Sturgeon, *Spectrochim. Acta. B.*, 2011, **66**, 594−603.
3. J. M. Symonds, A. S. Galhena, F. M. Fernández and T. M. Orlando, *Anal. Chem.*, 2010, **82**, 621−627.
4. G. C. Y. Chan, J. T. Shelley, J. S. Wiley, C. Engelhard, A. U. Jackson R. G. Cooks and G. M. Hieftje, *Anal. Chem.*, 2011, **83**, 3675−3686.
5. R. B. Cody, J. A. Laramée and H. D. Durst, *Anal. Chem.*, 2005, **77**, 2297−2302.
6. G. A. Harris, A. S. Galhena and F. M. Fernández, *Anal. Chem.*, 2011, **83**, 4508−4538.
7. G. J. Van Berkel, S. P. Pasilis and O. J. Ovchinnikova, *J. Mass Spectrom.*, 2008, **43**, 1161−1180.
8. D. J. Weston, *Analyst,* 2010, **135**, 661−668.
9. A. Venter, M. Nefliu and R. Graham Cooks, *TrAC Trends Anal. Chem*., 2008, **27**, 284−290.
10. J. D. Harper, N. A. Charipar, C. C. Mulligan, X. Zhang, R. G. Cooks and Z. Ouyang, *Anal. Chem.*, 2008, **80**, 9097−9104.
11. M. Siebenhaar, K. Küllmer, N. M. Fernandes, V. Hüllen and C. Hopf, *Anal. Bioanal. Chem*., 2015, **407**, 7229–7238.
12. K. J. Ewing, D. Gibson, J. Sanghera and F. Miklos, *Analytica Chimica Acta.,* 2015, **853**, 368–374.
13. 42. S. Gerbig, G. Stern, H. E. Brunn, R. Düring, B. Spengler and S. Schulz, *Anal. Bioanal. Chem*., 2017, **409**, 2107–2117.
14. X. W. Fang, S. P. Yang, K. Chingin, L. Zhu, X. L. Zhang, Z. Q. Zhou and Z. F. Zhao, *Int. J. Environ. Res. Public Health,* 2016, **13**, 814–820.
15. T. Y. Li, L. S. Fan, Y. F. Wang, X. B. Huang, J. G. Xu, J. X. Lu, M. Zhang and W. Xu, *Anal. Chem.*, 2017, **89**, 453–1458.
16. O. P. Haefliger and N. Jeckelmann, *Rapid Commun. Mass Spectrom.*, 2007, **21**, 1361−1366.
17. Y. Bai, J. Zhang and H. Liu, *Anal. Bioanal. Chem*., 2012. **403**. 2307−2314.
18. J. M. Nilles, T. R. Connell and H. D. Durst, *Anal. Chem.*, 2009, **81**, 6744−6749.
19. X. W. Wang, J. F. Liu, C. C. Liu, J. Zhang, B. Shao, L. P. Liu and N. N. Zhang, *J. Chromatogr. A*., 2014, **1333**, 134–137.
20. J. Lojza, T. Cajka, V. Schulzova, K. Riddellova and J. Hajslova, *J. Separ. Sci*., 2012, **35**, 476−481.
21. L. Vaclavik, E. Capuano, V. Gokmen and J. Hajslova, *Food Chem*., 2015, **173**, 290−297.
22. K. T. Upton, K. A. Schilling and J. L. Beauchamp, *Anal. Methods*, 2017, **9**, 5065.

23. Z. Takats, I. Cotte-Rodriguez, N. Talaty, H. Chen and R. G. Cooks, *Chem. Commun*., 2005, 1950−1952.

24. S. Yang, J. Ding, J. Zheng, B. Hu, J. Li, H. Chen, Z. Zhou and X. Qiao, *Anal. Chem*., 2009, **81**, 2426−2436.

25. H. Chen, J. Zheng, X. Zhang, M. Luo, Z. Wang and X. Qiao, *J. Mass. Spectrom.,* 2007, **42**, 1045−1056.

26. C. N. McEwen, R. G. McKay and B. S. Larsen, *Anal. Chem*., 2005, **77**, 7826−7831.

27. C. N. McEwen, in Encyclopedia of Analytical Chemistry (John Wiley & Sons, Ltd, 2006).

28. H. Wang, W. Sun, J. Zhang, X. Yang, T, Lina and Li Ding, *Analyst*, 2010. **135**. 688−695.

29. H. Wang, Y. Wu, B. Guo, W. Sun, L. Ding and B. Chen, *Analyst*, 2012, **137**, 3982−3988.

30. F. J. Andrade, J. T. Shelley, W. C. Wetzel, M. R. Webb, G. Gamez, S. J. Ray and G. M. Hieftje, *Anal. Chem*., 2008, **80**, 2646−2653.

31. M. C. Jecklin, G. Gamez, D. Touboul and R. Zenobi, *Rapid Commun. Mass Spectrom.*, 2008, **22**, 2791−2798.

32. J. T. Shelley, J. S. Wiley and G. M. Hieftje, *Anal. Chem*., 2011, **83**, 5741−5748.

33. L. V. Ratcliffe, F. J. M. Rutten, D. A. Barrett, T. Whitmore, D. Seymour, C. Greenwood, Y. Aranda-Gonzalvo, S. Robinson and M. McCoustra, *Anal. Chem*., 2007, **79**, 6094−6101.

34. T. L. Salter, F. M. Green, N. Faruqui and I. S. Gilmore, *Analyst*, 2011, **136**, 3274−3280.

35. N. Na, M. Zhao, S. Zhang, C. Yang and X. Zhang, *J. Am. Soc. Mass Spectrom.*, 2007, **18**, 1859−1862.

36. N. Na, C. Zhang, M. Zhao, S. Zhang, C. Yang, X. Fang and X. Zhang, *J. Mass Spectrom.*, 2007, **42**, 1079−1085.

37. M. J. Stein, E. Lo, D. G. Castner and B. D.Ratner, *Anal. Chem*., 2012, **84**, 1572−1578.

38. Y. Zhang, X. Ma, S. Zhang, C. Yang, Z. Ouyang and X. Zhang, *Analyst*, 2009, **134**, 176−181.

39. X. Zhan, Z. Zhao, X. Yuan, Q. Wang, D. Li, H. Xie, X. Li, M. Zhou and Y. Duan, *Anal. Chem*., 2013, **85**, 4512−4519.

40. D. Li, Y. H. Tian, Z. Zhao, W. Li and Y. Duan, *J. Mass Spectrom.*, 2015, **50**, 388−395.

41. Z. Zhao, D. Li, B. Wang, X. Ding, J. Dai, X. Yuan, X. Li and Y. Duan, *Int. J. Mass Spectrom.*, 2015, **376**, 65−74.

42. X. Ding, X. Zhan, X. Yuan, Z. Zhao and Y. Duan, *Anal. Chem*., 2013, **85**, 9013−9020.